INSTITUTE OF PHYSICS PUBLISHING JOURNAL OF PHYSICS: CONDENSED MATTER

J. Phys.: Condens. Matter **15** (2003) S2473–S2488 PII: S0953-8984(03)64561-3

A transport approach to the superconducting proximity effect in carbon nanotubes

J González

Instituto de Estructura de la Materia, Consejo Superior de Investigaciones Científicas, Serrano 123, 28006 Madrid, Spain

E-mail: imtjg64@pinar2.csic.es

Received 6 June 2003, in final form 16 July 2003
Published 15 August 2003
Online at stacks.iop.org/JPhysCM/15/S2473

Abstract

A microscopic approach is developed to account for the magnitudes of the supercurrents observed experimentally in carbon nanotubes placed between superconducting contacts. We build up a model for the nanotube ropes encompassing the electron repulsion from the Coulomb interaction and the effective attraction given by phonon exchange. We show that the available experimental data are consistent with the expected decay of the supercurrents along the length of the nanotube samples. Our results stress that propagation of Cooper pairs is favoured in the thick ropes, as a consequence of the reduction in the strength of the Coulomb interaction from the electrostatic coupling between the metallic nanotubes. We also provide an explanation for the temperature dependence of the supercurrents observed in the experiments, noting the existence of a crossover from a very flat behaviour at low temperatures to a pronounced decay in the long nanotubes.

1. Introduction

Since their discovery in 1991, carbon nanotubes have shown remarkable electronic properties. They may display quite different behaviours, depending on their geometry and the quality of the contacts used to probe the electronic transport. It was first predicted [1–3], and later checked experimentally [4, 5], that the nanotubes have semiconducting or metallic behaviour depending on the helicity of the hexagonal carbon rings wrapped around the tubule. This is the kind of versatility that indicates the carbon nanotubes to be ideal molecules for use in building electronic devices at the nanometre scale [6].

The electron correlations are moreover very strong in the carbon nanotubes, which leads to the breakdown of the conventional picture of electronic transport at low energies. Coulomb interaction prevails in the individual nanotubes [7, 8], and it drives the electron system to a state with the properties of the so-called Luttinger liquid, characterized by the absence of quasiparticles at the Fermi level. This feature is reflected in the power-law behaviour of

observables such as the tunnelling density of states, whose suppression at low energies has been actually observed in measurements of the conductance in carbon nanotubes [9, 10].

There have also been experiments revealing the existence of superconducting correlations in the nanotubes [11, 12]. The first observations were made on nanotube ropes suspended between superconducting electrodes, the most remarkable signal being the appearance of supercurrents for temperatures below the critical value of the contacts [11]. What was measured in that experiment was the proximity effect, by which Cooper pairs are formed in the nanotubes near the superconducting contacts. Later, superconducting transitions were observed in ropes suspended between metallic, nonsuperconducting electrodes [13]. The measurements reported in [13] indicate the existence of a superconducting phase intrinsic to the carbon nanotubes. More recently, strong superconducting correlations have also been reported in individual nanotubes of very small radius, inserted in a zeolite matrix [14].

The observation of superconducting correlations in the nanotubes implies that there is a regime which is different to that marked by the dominance of the Coulomb interaction. The appearance of superconducting effects requires a suitable attenuation of the repulsive interaction within the nanotubes, due to either the electrostatic coupling among the metallic nanotubes in a rope or the coupling with nearby conductors. Another factor that seems to be crucial is the achievement of high-quality contacts between the nanotubes and the electrodes. This has been possible in the experiments described in [11] by the use of a technique that allows one to solder and suspend the nanotubes between the contacts. The electrodes were made of a Re/Au bilayer (with transition temperature $T_c \approx 1.1$ K) in the case of a massive rope, and of a Ta/Au bilayer (with $T_c \approx 0.4$ K) in the case of a thin rope. The room temperature resistance of the ropes was consistent in each case with a resistance of the constituent metallic nanotubes below $h/e^2 \approx 25.8\,\mathrm{k}\Omega$ [11], which is of the order of the value $h/4e^2$ corresponding to ballistic transport in a nanotube.

Below the transition temperature of the contacts, the nanotubes can support currents without developing any resistance [11]. These so-called supercurrents reach a maximum value I_c, which is known as the critical current. This has been measured for the samples described in [11] and, as pointed out there, the magnitudes and temperature dependences obtained cannot be understood in the framework of the conventional proximity effect. The critical current is usually related to the values of the normal resistance R_N and the energy gap Δ in the superconductor through the expression $I_c = (\pi/2)\Delta/eR_N$. However, the value estimated in this way turns out to be about 40 times smaller than the experimental measurement for the thin rope reported in [11]. The observed dependence of the critical current on temperature is also very flat in that sample, before getting close to the transition temperature of the electrodes. This is again at odds with the conventional picture, in which the critical current should reflect the temperature dependence of the superconducting gap at the contacts.

A consistent explanation of the behaviour of the supercurrents measured experimentally has been proposed in [15]. It was stressed there that it is necessary to consider the supercurrents as an effect of one-dimensional (1D) transport along the carbon nanotubes. The propagation of the Cooper pairs in the nanotubes is favoured in the thick ropes, as there is a larger attenuation in the strength of the Coulomb interaction for higher content of metallic nanotubes in a rope [16]. The origin of this effect is similar to that of screening in a three-dimensional (3D) conductor. In a rope, however, the amplitude of tunnelling between neighbouring metallic nanotubes is highly suppressed in general, due to the misalignment of the respective carbon lattices [17, 18]. The absence of a significant intertube electron hopping is what keeps the Coulomb interaction long ranged in the nanotubes, despite the large reduction of its strength in the thick ropes.

In the present paper, we confront the results obtained using a microscopic model of the nanotube ropes with the experimental measurements from [11]. The propagation of the Cooper

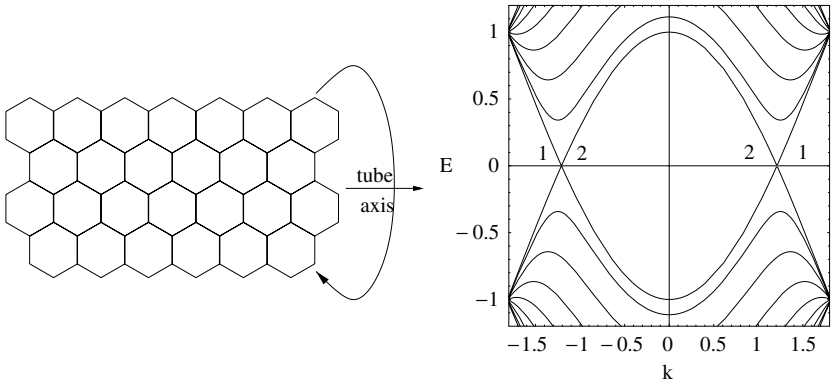

Figure 1. Left: a schematic representation of the wrapping action leading to an armchair nanotube. Right: the band structure of an armchair nanotube with nine subbands. The energy is measured in units of the overlap integral and the momentum in units of the inverse of the C–C distance.

pairs along the carbon nanotubes gives rise to supercurrents with a strong dependence on the length of the junction, when the Coulomb interaction prevails in the electron system. Thus, the measurements of the supercurrents, available for two experimental samples with different lengths and contents of the metallic nanotubes, can be used to discern the character of the interactions present in the nanotubes. We will see, in particular, that the value of the critical current in the thin rope reported in [11] can be accounted for by considering an attractive component in the electron–electron interaction, coming from the coupling of the electrons to the elastic modes of the carbon lattice. In general, the balance between the renormalized Coulomb interaction in the ropes and the attractive component of the interaction allows us to explain the magnitudes as well as the temperature dependence of the critical currents reported in [11].

In the next section, we review the different sources of electron–electron interaction in the carbon nanotubes and describe the microscopic model relevant for the nanotube ropes. Section 3 is devoted to setting up the framework used for the study of transport along the junctions. The comparison between the results from the microscopic model and the experimental data is carried out in section 4. Finally, the conclusions from our investigation are drawn in section 5.

2. Electronic interactions in carbon nanotubes

We review first the structure of the modes and interactions that take place at low energies in carbon nanotubes. The band structure, for all the metallic nanotubes, has two pairs of linear branches that cross at opposite Fermi points (for undoped nanotubes) as shown in figure 1. The metallic nanotubes found in the ropes have typically a radius R around $\approx$0.7 nm, and their electron modes in the energy range below $\approx$0.5 eV belong to the linear branches near the Fermi level, as can be seen from figure 1. Therefore, we will pay attention just to them when studying the low-energy properties of the carbon nanotubes.

We will proceed with a discussion throughout this section having in mind the specific geometry of the armchair nanotubes, illustrated in figure 1, while a completely parallel construction can be carried out for the metallic chiral nanotubes. The linear branches found near the Fermi level can be divided into two classes, according to the different symmetries of their modes under the exchange of the two sublattices of the hexagonal carbon lattice.

In the case of armchair nanotubes, the two subbands that cross at the Fermi level, labelled 1 and 2 in figure 1, correspond to the eigenvalues of the one-particle Hamiltonian

$$\mathcal{H} = t \begin{pmatrix} 0 & 1 - 2\cos(\sqrt{3}ka/2) \\ 1 - 2\cos(\sqrt{3}ka/2) & 0 \end{pmatrix} \tag{1}$$

that operates in the space of the electron amplitudes in the two different atoms of the lattice basis [19]. The parameter t represents the matrix element of the potential for nearest-neighbour carbon orbitals and a is the C–C distance. Then, it is clear that the modes in subband 1 have a smooth amplitude in the carbon lattice, while the modes in subband 2 have an amplitude that alternates in sign when shifting between nearest-neighbour atoms. This has important consequences regarding the form of the interactions between the different branches.

2.1. Coulomb interactions

The Coulomb interaction provides a strong source of repulsion between the electrons in the carbon nanotubes. One may obtain an effective 1D potential $V_{\mathrm{C}}(x - x')$ on the longitudinal dimension of the nanotube, by taking the average of the 3D interaction over two nanotube sections placed at a spatial separation $x - x'$ [8]. The Fourier transform with respect to this variable gives a potential which is logarithmically singular for small momentum transfer k [20],

$$V_{\mathrm{C}}(k) = (e^2/2\pi) \log |(k_{\mathrm{c}} + k)/k|. \tag{2}$$

The large momentum k_{c}, of the order of $\sim 1/R$, survives in the projection onto the longitudinal dimension as a remnant of the finite radius of the nanotube.

In fact, the Coulomb interaction remains singular only when acting between currents that belong each to a given linear branch. Otherwise, if one of the electron modes is scattered to another branch with different symmetry in the two-atom basis, the product of the *in* and *out* amplitudes has alternating sign over the hexagonal carbon lattice. Then, the scattering amplitude averages to zero when making the 1D projection with a large spatial separation $x - x'$ along the nanotube.

At short distances, the Coulomb interaction may still give rise to a residual 1D interaction mixing *in* and *out* modes in different linear branches, but these processes do not bear the singular character of the long-range interaction. This also applies to the processes with large momentum transfer in which the electron modes are scattered from one of the Fermi points to the other. These backscattering and Umklapp processes have a strength which is reduced by a factor of the order of $\sim 0.1a/R$ with respect to the nominal strength $e^2/2\pi$ of the long-range Coulomb interaction [7, 8]. For nanotubes with $R \approx 0.7$ nm, that factor has a magnitude of ~ 0.01. Thus, the backscattering and Umklapp interactions of this kind turn out to be negligible in comparison to the Coulomb interaction between currents in definite linear branches.

2.2. Electron–phonon interactions

Another source of electron–electron interaction comes from the coupling of the electrons to the elastic modes of the carbon lattice. The exchange of phonons gives rise to a retarded interaction, which can be represented in terms of an effective potential $V(k, \omega)$ depending on the frequency ω and the phonon momentum k [21]. In the case of carbon nanotubes, the potential can be expressed in the form

$$V(k, \omega) = -g_{p,p'}(k) g_{q,q'}(-k) \frac{\omega_k}{-\omega^2 + \omega_k^2} \tag{3}$$

where ω_k is the phonon energy and the $g_{p,p'}(k)$ are the electron–phonon couplings, with indices p and p' labelling the gapless subbands to which the *in* and *out* electron modes belong.

Thus, for frequencies ω below the characteristic phonon energies, the potential $V(k, \omega)$ may reach negative values, providing then a kind of effective attraction between the electrons.

For the computation of the $g_{p,p'}(k)$, we rely on the tight-binding approximation, which is fairly appropriate for the carbon nanotubes. The electron–phonon couplings can be represented by a sum over nearest neighbours of the atoms in the unit cell of the nanotube [22]

$$g_{p,p'}(k-k') = \frac{1}{(\mu\omega_{k-k'})^{1/2}} \sum_{\langle s,s'\rangle} u_s^{(p)*}(k) u_{s'}^{(p')}(k')(\boldsymbol{\epsilon}_s(k-k') - \boldsymbol{\epsilon}_{s'}(k-k')) \cdot \boldsymbol{\nabla} J(s,s') \qquad (4)$$

where $\boldsymbol{\epsilon}_s(k-k')$ is the phonon polarization vector at site s, $u_{s'}^{(p')}(k')$ and $u_s^{(p)}(k)$ are the respective amplitudes of the incoming and outgoing electrons, $J(s,s')$ is the matrix element of the potential between orbitals at s and s', and μ is the mass per unit length. We are already implying that the coupling can be expressed as a function of $k-k'$, which is a reasonable approximation for small values of that momentum transfer (modulo $2k_F$).

The product of the two couplings in (3) can be actually positive or negative, depending on the linear branches involved [22]. The sign is dictated by symmetry rules which are direct consequences of the geometry of the nanotube lattice, as can be illustrated in the particular case of the armchair nanotubes. Thus, taking into account that the modes with antibonding character have an amplitude with alternating sign in nearest-neighbour sites, we observe from inspection of (4) that

$$g_{1,1}(k) = -g_{2,2}(k). \qquad (5)$$

The electrons can be also scattered from one of the subbands to the other by exchanging phonons. The fact that one of the modes has then antibonding character is reflected in the antisymmetric condition

$$g_{1,2}(k) = -g_{2,1}(k). \qquad (6)$$

The relations (5) and (6) are based on symmetry rules, and they hold irrespective of whether the exchanged phonons are optical or acoustic.

In the more general case of chiral metallic nanotubes, it can be shown by means of similar arguments that the constraints (5) and (6) still hold for the two gapless subbands. These correspond to the different eigenvalues of a one-particle Hamiltonian such as (1), whose eigenvectors bind the relative electron amplitudes in the two atoms of the lattice basis [19]. Their respective expressions for the two linear branches at each Fermi point have in general the form

$$\begin{pmatrix} 1 \\ e^{i\phi} \end{pmatrix}, \qquad \begin{pmatrix} 1 \\ -e^{i\phi} \end{pmatrix}, \qquad (7)$$

where ϕ is an angle that vanishes for armchair nanotubes and equals $\pi/2$ for zigzag nanotubes. Given that the difference between the two eigenvectors is just the minus sign in the lower component, it can be checked that the exchange of the gapless subbands in the computation of the electron–phonon couplings leads in general to the relations (5) and (6).

Using the fact that $g^*_{p,p'}(k-k') = g_{p',p}(k'-k)$, it is clear from (3) that the exchange of phonons gives rise to an attractive electron–electron interaction when the electrons are scattered within the same subband. On the other hand, the condition (5) on the couplings makes the interaction repulsive between electron currents in different subbands. These considerations hold for frequencies below the typical Debye energy of the phonons, which is in the range between 0.1 and 0.2 eV for nanotubes with radius around $\approx$0.7 nm [23–25]. Taking into account these magnitudes and that the variation of the matrix element J with the C–C distance is given by $\partial J/\partial a \approx 4.5$ eV Å^{-1}, one can make an estimate of the strength of the effective interaction. In units in which $\hbar = 1$, the values of the potential (3) can be naturally compared

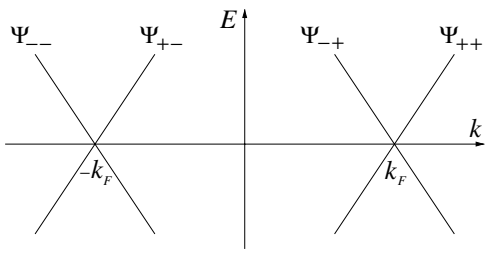

Figure 2. Linear branches and the respective electron fields in the low-energy spectrum of a metallic nanotube.

to the Fermi velocity v_{F} in the carbon nanotubes. The strength of the effective interaction is given by $(\partial J/\partial a)^2/\mu\omega_k^2$, which turns out to be of the order of $0.1v_{\mathrm{F}}$, with $v_{\mathrm{F}} \approx 8 \times 10^5$ m s^{-1}.

2.3. Low-energy dynamics

When describing the low-energy dynamics of the electrons, one has to bear in mind the special structure of the nanotube ropes. These are made of a disordered mixture of nanotubes with different helicities and diameters. In these conditions, the tunnelling of electrons between neighbouring metallic nanotubes is highly suppressed. This comes from the fact that the carbon lattices of neighbouring nanotubes are not aligned in general, which leads to a mismatch between the respective Fermi points and to the consequent difficulty of conserving the longitudinal momentum in the tunnelling process [17]. An experimental signature of the very small tunnelling amplitude has been observed in the measurement of the coupling resistance between tubes, which has shown wide variations ranging between 2 and 140 MΩ in different samples [18]. This is consistent with a picture in which the amplitude of the tunnelling between nanotubes may be about three orders of magnitude below the electron hopping amplitude within the carbon lattice. We will therefore assume that the coupling between nanotubes is given by the Coulomb interaction, and that the kinetic energy of the electrons can be represented by the sum of the kinetic energies of the metallic nanotubes in the rope.

Within each nanotube, one has to balance the repulsive Coulomb interaction and the effective electron–electron interaction coming from phonon exchange. As remarked above, there are no significant backscattering or Umklapp processes coming from the Coulomb interaction, so the competition between that and the effective attraction takes place in processes where the scattered electrons remain in their respective branches. Our approach will focus on the description of this balance between repulsive and attractive interactions. For that purpose, we will build a model in which the elementary objects are the electron density operators, given in terms of the Fermi fields $\Psi^{(a)}_{ri\sigma}(x)$ for the different linear branches (shown in figure 2) by

$$\Psi^{(a)\dagger}_{ri\sigma}(x)\Psi^{(a)}_{ri\sigma}(x) = \rho^{(a)}_{ri\sigma}(x). \tag{8}$$

The label a runs over the different metallic nanotubes in a rope, $a = 1, \ldots, n$. The index $r = \pm$ is used as a label to indicate the left- or right-moving character of the linear branch, and the index $i = \pm$ as a label to indicate the Fermi point. The index σ stands for the two different spin projections. In this way, we are setting aside the backscattering processes, which tend anyhow to enhance the superconducting correlations [26]. Then, it can be thought that our model leads to a slight underestimation of these effects, for a given strength of the bare attractive interaction. This can be corrected by a suitable renormalization of the effective coupling derived from phonon exchange, assuming that it reaches greater values in the low-energy regime of the model [27].

According to the above considerations, we write the Hamiltonian for a nanotube rope in the form

$$H_0 = \tfrac{1}{2} v_{\mathrm{F}} \int_{-k_{\mathrm{c}}}^{k_{\mathrm{c}}} \mathrm{d}k \sum_{ari\sigma} :\rho^{(a)}_{ri\sigma}(k)\rho^{(a)}_{ri\sigma}(-k): + \tfrac{1}{2} \int_{-k_{\mathrm{c}}}^{k_{\mathrm{c}}} \mathrm{d}k \sum_{ari\sigma} \rho^{(a)}_{ri\sigma}(k) \sum_{bsj\sigma'} V^{(ab)}_{ri,sj}(k)\rho^{(b)}_{sj\sigma'}(-k). \quad (9)$$

The first term in (9) comes from the known representation of the kinetic energy for a 1D electron system [28, 29]. The potential $V^{(ab)}_{ri,sj}(k)$ mediates the interactions within a given nanotube for $a = b$ and between different nanotubes for $a \neq b$. Due to the long-range character of the Coulomb interaction, its contribution has to be included in all the elements $V^{(ab)}$. It is only for $a = b$, however, that one has to add the contributions arising from phonon exchange within each nanotube.

We can introduce two plausible assumptions that lead to a straightforward resolution of the model under study. The first is that all the relevant interactions in the nanotube system are spin independent. This certainly applies to the long-range Coulomb interaction, which has the same strength irrespective of whether the electron currents have parallel or antiparallel spins. Regarding the effective interactions from phonon exchange, it is also clear from our description in the preceding subsection that they do not depend on the spin projection of the scattered electrons. Then, it is appropriate to introduce the symmetric and antisymmetric combinations of density operators for the two spin projections. Only the charge density operators

$$\rho^{(a)}_{ri\rho}(k) = \frac{1}{\sqrt{2}}(\rho^{(a)}_{ri\uparrow}(k) + \rho^{(a)}_{ri\downarrow}(k)) \quad (10)$$

enter in the interaction term of the Hamiltonian (9). This implies, in particular for the calculation of the correlators, that half of the degrees of freedom in the model are not affected by the interaction.

We will further assume that the strength of the effective interaction from phonon exchange does not depend on the particular linear branches to which the scattered electron modes belong. The amplitude of the scattering mediated by phonons can only have a significant dependence on the energy of the exchanged phonons, as observed in equations (3) and (4). That may lead one to distinguish in general between processes in which the momentum transfer is close to zero and near $2k_{\mathrm{F}}$. Regarding the superconducting effects, though, the most important role is played by the most energetic phonons, since the Debye frequency sets the energy range of the attractive interaction. At that scale, the energy of the optical phonons near zero momentum becomes comparable to the energy of phonons with momentum $2k_{\mathrm{F}}$. Then, it is justified to assume that the strength of the interaction processes relevant for the superconductivity cannot have a significant dependence on the momentum transfer of the interaction.

We know however that, if the exchange of phonons takes place between currents in different subbands, condition (5) introduces a relative minus sign. It is convenient to define the respective charge density operators for the bonding and the antibonding subband as

$$\tilde{\rho}^{(a)}_{1\rho}(k) = \rho^{(a)}_{++\rho}(k) + \rho^{(a)}_{--\rho}(k) \quad (11)$$

$$\tilde{\rho}^{(a)}_{2\rho}(k) = \rho^{(a)}_{+-\rho}(k) + \rho^{(a)}_{-+\rho}(k). \quad (12)$$

The Coulomb interaction always has repulsive character, and it acts on the symmetric combination of (11) and (12),

$$\tilde{\rho}^{(a)}_{+\rho}(k) = \frac{1}{\sqrt{2}}(\tilde{\rho}^{(a)}_{1\rho}(k) + \tilde{\rho}^{(a)}_{2\rho}(k)). \quad (13)$$

The effective interaction from phonon exchange is attractive between currents in the same subband, but repulsive for currents in different subbands. It therefore acts on the antisymmetric

combination

$$\tilde{\rho}^{(a)}_{-\rho}(k) = \frac{1}{\sqrt{2}}(\tilde{\rho}^{(a)}_{1\rho}(k) - \tilde{\rho}^{(a)}_{2\rho}(k)). \tag{14}$$

In the new density variables, the Hamiltonian can be written in the form

$$H_0 = \tfrac{1}{2} v_{\mathrm{F}} \int_{-k_{\mathrm{c}}}^{k_{\mathrm{c}}} \mathrm{d}k \sum_{ari\sigma} :\rho^{(a)}_{ri\sigma}(k)\rho^{(a)}_{ri\sigma}(-k): + \frac{1}{2}\int_{-k_{\mathrm{c}}}^{k_{\mathrm{c}}} \frac{\mathrm{d}k}{2\pi}\left(4\sum_a \tilde{\rho}^{(a)}_{+\rho}(k)V_{\mathrm{C}}(k)\sum_b \tilde{\rho}^{(b)}_{+\rho}(-k) + 4g\sum_a \tilde{\rho}^{(a)}_{-\rho}(k)\tilde{\rho}^{(a)}_{-\rho}(-k)\right) \tag{15}$$

where g (<0) parametrizes the strength of the effective interaction from phonon exchange. The Hamiltonian (15) encompasses the main interactions in the nanotube system, providing a suitable starting point for studying the superconducting correlations in the nanotube ropes.

3. Superconducting correlations and supercurrents in carbon nanotubes

We introduce in what follows the theoretical framework appropriate for the description of supercurrents in carbon nanotubes. The study of the Josephson effect in a Luttinger liquid placed between macroscopic superconductors has been pursued in [30] and [31]. We first review briefly the approach proposed in [31] for the calculation of the critical current through that kind of junction.

In order to describe the coupling to superconducting electrodes, one more term $H_{\mathrm{T}j}$ has to be added to the Hamiltonian of the 1D system for each of the tunnel junctions created at the contacts. The term $H_{\mathrm{T}j}$ expresses the hopping of electrons from the location d_j of the contact in the 1D system to the superconductor and vice versa, with a given tunnelling amplitude t_j. It then has the form

$$H_{\mathrm{T}j} = t_j \sum \Psi^{(a)\dagger}_{\sigma}(d_j)\Psi_{\mathrm{S}j,\sigma}(d_j) + \mathrm{h.c.} \tag{16}$$

where $\Psi_{\mathrm{S}j,\sigma}(d_j)$ is the electron field at the end of the superconductor Sj, and $\Psi^{(a)}_{\sigma}(d_j)$ is a generic electron field of the 1D system.

On top of that, one also has to include the Hamiltonians describing the condensates for the respective macroscopic superconductors. For our purposes, all the relevant information about their properties can be given in terms of the respective order parameters Δ_j and normal densities of states N_j at the contacts.

The supercurrent I through the 1D system can be computed in terms of the derivative of the free energy $\mathcal{F}$ with respect to the difference of the respective phases χ_1 and χ_2 of the order parameters in the two superconductors [31]. Using the notation $\chi = \chi_1 - \chi_2$, we have

$$I(\chi) = -2e\frac{\partial \mathcal{F}}{\partial \chi}. \tag{17}$$

When the junctions are not highly transparent, one can adopt a perturbative approach by expanding in powers of the tunnelling Hamiltonians $H_{\mathrm{T}j}$. For usual instances in which the time of propagation between the tunnel junctions is larger than $1/\Delta$, the contributions to the derivative in (17) are dominated by processes in which the Cooper pairs tunnel from one of the superconductors to the 1D system, propagating then to the other superconducting contact [31]. These first perturbative contributions give the result

$$I(\chi) \approx 8et_1^2t_2^2k_{\mathrm{B}}T \times \frac{\mathrm{d}}{\mathrm{d}\chi}\int_0^{1/k_{\mathrm{B}}T}\mathrm{d}\tau_1\int_0^{\tau_1}\mathrm{d}\tau_2\int_0^{\tau_2}\mathrm{d}\tau_3\int_0^{\tau_3}\mathrm{d}\tau_4\,\langle\Psi^{\dagger}_{\mathrm{S}1,\sigma}(d_1,-\mathrm{i}\tau_1)\Psi^{\dagger}_{\mathrm{S}1,-\sigma}(d_1,-\mathrm{i}\tau_2)\rangle$$

$$\times \langle \Psi^{(a)}_{\sigma}(d_1, -\mathrm{i}\tau_1)\Psi^{(a)}_{-\sigma}(d_1, -\mathrm{i}\tau_2)\Psi^{(a)\dagger}_{\sigma'}(d_2, -\mathrm{i}\tau_3)\Psi^{(a)\dagger}_{-\sigma'}(d_2, -\mathrm{i}\tau_4)\rangle$$
$$\times \langle \Psi_{\mathrm{S}2,\sigma'}(d_2, -\mathrm{i}\tau_3)\Psi_{\mathrm{S}2,-\sigma'}(d_2, -\mathrm{i}\tau_4)\rangle \tag{18}$$

where the statistical averages, at temperature T, are taken over ordered products with respect to imaginary time τ, in the respective systems of the fields.

At low enough temperatures, we can approximate the statistical averages at the boundary of the superconductors by delta functions in imaginary time:

$$\langle \Psi_{\mathrm{S}j,\sigma}(d_j, -\mathrm{i}\tau_1)\Psi_{\mathrm{S}j,-\sigma}(d_j, -\mathrm{i}\tau_2)\rangle \approx \mathrm{e}^{\mathrm{i}\chi_j} N_j \delta(\tau_1 - \tau_2), \tag{19}$$

χ_j being the phase of the order parameter in the superconductor Sj. Then the expression (18) is greatly simplified. The dependence of $I(\chi)$ on the phase difference χ arises after multiplying the exponentials of the respective phases χ_1 and χ_2, that appear in two-point correlators such as (19). After taking the derivative with respect to the phase difference, the resulting function $I(\chi)$ shows an oscillatory behaviour in the χ variable. We identify the maximum value of the function with the critical current $I_{\mathrm{c}}(T)$, which is given by

$$I_{\mathrm{c}}(T) \approx 2eN_1N_2t_1^2t_2^2 \int_0^{1/k_{\mathrm{B}}T} \mathrm{d}\tau\, \langle \Psi^{(a)}_{\sigma}(d_1, -\mathrm{i}\tau)\Psi^{(a)}_{-\sigma}(d_1, -\mathrm{i}\tau)\Psi^{(a)\dagger}_{\sigma'}(d_2, 0)\Psi^{(a)\dagger}_{-\sigma'}(d_2, 0)\rangle. \tag{20}$$

The expression of the critical current in (20) has been conveniently simplified by using the time-translational invariance of the four-point correlator to fix the time variable at one of the ends of the propagation, at the expense of multiplying by its range of integration $1/k_{\mathrm{B}}T$.

We now make the passage to applying the above approach to the case of the carbon nanotubes. The critical current in (20) is given in terms of the propagator of the Cooper pairs along the 1D system. We need therefore to compute that object with the fields corresponding to the linear branches crossing the Fermi level of the carbon nanotubes, in the model governed by the Hamiltonian (15).

The calculation of the 1D correlators can be accomplished by making use of bosonization techniques [28, 29]. For each linear branch of the carbon nanotubes, one can define a boson operator $\Phi^{(a)}_{ri\sigma}(x)$, related to the respective electron density operator by

$$\partial_x \Phi^{(a)}_{ri\sigma}(x) = 2\pi\rho^{(a)}_{ri\sigma}(x). \tag{21}$$

The bosonization method relies on the feasibility of expressing the fermion fields in terms of the respective boson operators:

$$\Psi^{(a)}_{\pm i\sigma}(x) = \frac{1}{\sqrt{\alpha_{\mathrm{c}}}} \exp(\pm\mathrm{i}\Phi^{(a)}_{\pm i\sigma}(x)), \tag{22}$$

α_{c} being a short-distance scale which appears also in the mode expansion for the boson fields [28]. Usually, these are cut off smoothly by insertion of the factor $\exp(-\alpha_{\mathrm{c}}k)$ in the integration over modes. In our description, we have preferred to instead place a sharp limit on the momentum integrals, led by the fact that the nanotubes have a finite transverse size. It is clear however that the two schemes have to give in essence the same results, when the appropriate correspondence with $\alpha_{\mathrm{c}} \approx k_{\mathrm{c}}^{-1}$ is established between them.

In the case of the carbon nanotubes, the propagator that enters in the computation of the critical current in (20) is of the type

$$G(x, t) \equiv \langle \Psi^{(a)\dagger}_{++\uparrow}(0, 0)\Psi^{(a)\dagger}_{--\downarrow}(0, 0)\Psi^{(a)}_{--\downarrow}(x, t)\Psi^{(a)}_{++\uparrow}(x, t)\rangle \tag{23}$$

where the choice of linear branches accounts for the fact that the Cooper pairs are formed with zero total momentum. The evaluation of (23) can be done by using the bosonization formulae (22) and passing to the combination of boson fields that bring the Hamiltonian (15) into diagonal form.

The Hamiltonian (15) already exhibits a natural separation between the respective sectors for the symmetric and the antisymmetric combination of electronic charge in the two gapless subbands. In order to write it as a diagonal quadratic form, one has to change to a set of variables given by the totally symmetric combination of charge density operators $\tilde{\rho}^{(a)}_{+\rho}(k)$ for the n metallic nanotubes, plus $n-1$ suitable antisymmetric combinations of the same operators, defined such that the new variables all remain mutually orthogonal. We observe from (15) that the Coulomb interaction acts only on the totally symmetric combination of charge density operators $\tilde{\rho}^{(a)}_{+\rho}(k)$. Thus, the repulsive interaction is only felt in one out of the $4n$ possible interaction channels. These arise from the n different metallic nanotubes and the degeneracy in the gapless subbands and spin projections, and they can be classified into the respective sectors for the $\tilde{\rho}^{(a)}_{+\rho}(k)$ and the $\tilde{\rho}^{(a)}_{-\rho}(k)$ operators, and similar sectors which take into account the spin density operators.

Expressions for correlators such as (23) factorize into contributions for each of the different interaction channels that are found in the diagonal expression of the Hamiltonian. That is, the propagator for the Cooper pairs can be written in the form

$$G(x,t) = \frac{1}{\alpha_{\mathrm{c}}^2} C(x,t) \prod_{1}^{n} N(x,t) \prod_{1}^{3n-1} F(x,t). \tag{24}$$

The first factor comes from the propagation of the total charge density from all the metallic nanotubes, which has a purely electrostatic interaction. The next n equivalent factors stand for the contribution of the charge mismatch in the gapless subbands, which bears the effect of the attractive interaction according to (15). The remaining $3n-1$ factors account for the free propagation of the rest of the density excitations, including the spin degrees of freedom and charge degrees of freedom orthogonal to those affected by the interaction.

Each of the factors in (24) corresponds to the propagation of a boson field. At zero temperature, for instance, all of them adhere to the common expression

$$X(x,t) = \exp\left(-\frac{1}{2n} \int_0^{k_{\mathrm{c}}} \mathrm{d}k \, \frac{1}{\mu(k)k} (1 - \cos(kx)\cos(\tilde{v}_{\mathrm{F}} k t)) \right). \tag{25}$$

The respective quantities $\mu(k)$ arise in the change of variables that makes the Hamiltonian (15) diagonal. This process also leads to a renormalization of the respective Fermi velocities, given by $\tilde{v}_{\mathrm{F}}(k) = v_{\mathrm{F}}/\mu(k)$. In the case of $C(x,t)$, we have $\mu(k) = 1/\sqrt{1 + 4nV_{\mathrm{C}}(k)/\pi v_{\mathrm{F}}}$, while for $N(x,t)$ the quantity $\mu(k)$ does not depend on the momentum, $\mu = 1/\sqrt{1 - 4|g|/\pi v_{\mathrm{F}}}$. For the rest of excitations with free propagation, we simply have $\mu(k) = 1$ and $\tilde{v}_{\mathrm{F}}(k) = v_{\mathrm{F}}$.

In practice, one is interested in the behaviour of the supercurrents at finite temperature, which requires moreover the knowledge of the propagator (23) at imaginary time. For this reason, it is more appropriate to deal with the representation of objects such as (25) at finite temperature in the Matsubara formalism, introducing the sum over discrete frequencies $\omega_m = 2\pi m k_{\mathrm{B}} T$:

$$X(x, -\mathrm{i}\tau) = \exp\left(-\frac{1}{2n} \int_0^{k_{\mathrm{c}}} \mathrm{d}k \, \frac{2k_{\mathrm{B}}T}{v_{\mathrm{F}}} \sum_{m=-\infty}^{m=+\infty} \frac{1 - \cos(kx)\cos(\omega_m \tau)}{(\omega_m/\tilde{v}_{\mathrm{F}})^2 + k^2} \right). \tag{26}$$

Thus, the framework developed is well suited to discussion of the behaviour of the supercurrents in carbon nanotubes depending on the temperature T, the distance $d_1 - d_2$ between the superconducting contacts, the number n of metallic nanotubes in a rope, and the competition between the repulsion given by the Coulomb interaction and the effective attraction given by phonon exchange.

4. Comparison with experimental data

In this section we establish the comparison with the experimental measurements of supercurrents in carbon nanotubes reported in [11]. The supercurrents were observed in two nanotube samples with different structure. One of them consisted of a rope containing approximately 200 nanotubes, with a length of about 1.7 μm. The other sample was made of seven tubes merging at one of the ends into a single nanotube, extending to a total length of 0.3 μm. It has been remarked in [11] that the critical current $I_c \approx 0.1$ μA measured in the thin rope was about 40 times larger than expected within the conventional framework of the proximity effect. The very flat shape of the critical current as a function of the temperature was also surprising, as its decay was only apparent in the neighbourhood of the critical temperature for the superconducting electrodes. The thick rope showed a more conventional behaviour, although the decay of the supercurrent at the critical temperature of the electrodes was not as sharp as expected [11].

We face the challenge of accounting for the experimental values and features of the critical currents with our microscopic model, that allows us to describe ropes with any kind of nanotube content. In this respect, our computational framework has only a few adjustable parameters. The prefactors that affect the strength of the critical current in (20) can be encoded into the relative conductances G_i at the tunnel junctions, given (in units of $4e^2$) by $G_i = N_i t_i^2/v_F$. The critical current gets the right dimensions from the combination ev_Fk_c, that arises after setting $\alpha_c^{-1} = k_c$ and performing the integral in (20) over the dimensionless variable $\tilde{\tau} = v_Fk_c\tau$. The expression of the critical current becomes

$$I_c(T) \approx 2G_1G_2ev_Fk_c \int_0^{v_Fk_c/k_BT} d\tilde{\tau}\, C(L, -i\tilde{\tau}/v_Fk_c) \prod_1^n N(L, -i\tilde{\tau}/v_Fk_c) \times \prod_1^{3n-1} F(L, -i\tilde{\tau}/v_Fk_c) \tag{27}$$

where L represents the distance between the superconducting contacts.

Equation (27) gives the critical current per metallic nanotube in a rope. We observe that the order of magnitude is given at short distances by the quantity ev_Fk_c. It is reasonable to set the short-distance cut-off according to the scale of the nanotube diameter, and we will take $k_c \approx 0.25$ nm^{-1} for typical nanotubes in a rope. This sets a unit scale $ev_Fk_c \approx 15$ μA for the critical currents in carbon nanotubes.

One has to bear in mind, however, that the critical currents obtained from (27) display a strong dependence on the distance between superconducting contacts. Their decay for increasing length L can be very pronounced in ropes with a small number of metallic nanotubes, where the electron interactions are predominantly repulsive. The behaviour at large L becomes much softer in the thick ropes, as shown in figure 3. In general, the decay of the critical currents with the length L is not given by a simple power law, since the dependence of the Coulomb potential $V_C(k)$ on the momentum prevents perfect scaling of the observables at long distances.

The results shown in figure 3 allow us to draw a comparison with the values of the critical currents at $T \approx 0$ K reported in [11]. The appropriate correspondence with the thin rope described there is established by making the reasonable assumption that two out of the seven nanotubes in the rope are metallic. Moreover, we determine the theoretical value of the critical current by looking at the decay along the distance between the contacts, setting $L = 75/k_c$ for the thin rope. For that choice of the parameters and taking a strength $2e^2/\pi^2v_F = 1.0$ for the Coulomb interaction, we observe that the experimental value of the critical current ($I_c \approx 0.1$ μA) can be matched by taking a coupling for the attractive interaction $g/\pi v_F = 0.2$.

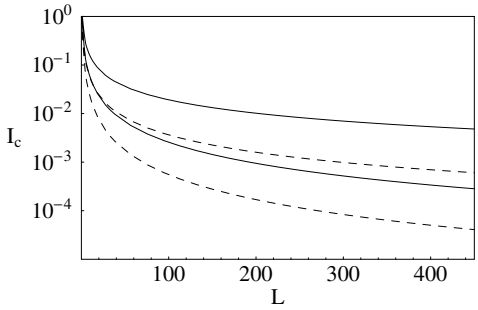

Figure 3. Plots of the critical current per metallic nanotube (measured in units of $ev_F k_c$, which we take as $\approx$15 μA) versus distance between the superconducting contacts (in units of k_c^{-1}) at $T = 0$. The full curves represent the results for ropes with a number of metallic nanotubes $n = 60$ (top) and $n = 2$ (bottom), taking $2e^2/\pi^2 v_F = 1.0$ and a strength of the effective attractive interaction $g/\pi v_F = 0.2$. The dashed curves represent the respective counterparts for the same values of n in the absence of attractive interaction.

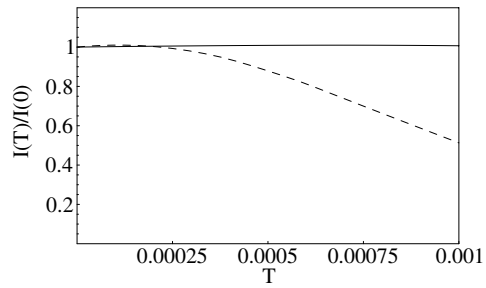

Figure 4. Plots of the normalized values of the critical current versus temperature (measured in units of $v_F k_c/k_B$) in a thin rope with two metallic nanotubes, for $2e^2/\pi^2 v_F = 1.0$, $g/\pi v_F = 0.2$, and respective nanotube lengths $L = 75/k_c$ (full line) and $L = 425/k_c$ (dashed curve).

In fact, the value of the integral in (27) at zero temperature for $n = 2$ and $L = 75/k_c$ is $\approx 3.8 \times 10^{-3}$, which gives a critical current $2I_c(0) \approx 0.11$ μA (times $2G_1G_2$) after adding the contributions of the two metallic nanotubes.

The precise determination of the critical current is affected by the values of the relative conductances G_1 and G_2. It is however reassuring that, once the interaction strengths are fixed to the above mentioned values, one can reproduce approximately the ratio between the critical currents observed in the two different samples where the supercurrents have been measured. In the case of the thick rope, we assume that it may have a number of metallic nanotubes $n \approx 60$, and we estimate the critical current by computing the decay for a rope 1.7 μm long, which corresponds to $L = 425/k_c$ in our model. The value of the integral in (27) at zero temperature for $n = 60$ and $L = 425/k_c$ is $\approx 5.1 \times 10^{-3}$. This leads us to the result that the critical current in the thick rope should be about 40 times greater than that in the thin rope, taking into account the approximate ratio between the number of metallic nanotubes in the two samples. This agrees well with the order of magnitude of the experimental value $I_c \approx 2.5$ μA for the thick rope reported in [11].

The other important check is that our model is able to account for the dependence of the critical currents on temperature observed experimentally. We have represented in figure 4 the behaviour obtained from (27), computing now the critical current at a fixed distance $L = 75/k_c$,

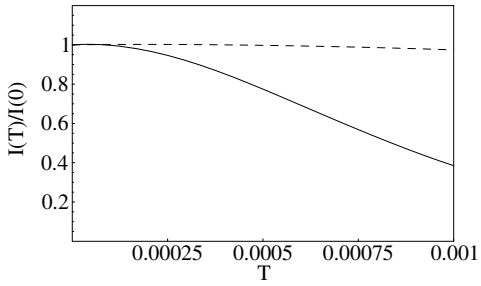

Figure 5. Plots of the normalized values of the critical current versus temperature (measured in units of $v_F k_c/k_B$) in a thick rope with 60 metallic nanotubes, for $2e^2/\pi^2 v_F = 1.0$, $g/\pi v_F = 0.125$, and respective nanotube lengths $L = 425/k_c$ (full curve) and $L = 75/k_c$ (dashed line).

for the thin rope with $n = 2$ (and keeping a suitable value of the coupling $g/\pi v_F = 0.2$). The temperature is measured in units of $v_F k_c/k_B \approx 1.2 \times 10^3$ K. Thus, in the case of the thin rope, the transition temperature $T_c \approx 0.4$ K of the superconducting contacts corresponds to a value $k_B T_c/v_F k_c \approx 3 \times 10^{-4}$ on the scale of figure 4. We observe that the natural behaviour of the critical current is being flat over such range of small temperatures, in agreement with the experimental measurements in the thin rope studied in [11]. The present results can be trusted while remaining away from the critical temperature T_c of the superconducting electrodes, as we have not paid attention to the dependence of their gaps on temperature. The sharp decay of the critical current observed experimentally near T_c is just the natural consequence of approaching the superconducting transition of the contacts.

We have to remark, however, that the flat behaviour of the critical current as a function of T is a consequence of the short distance along which it has been measured in the thin rope. For long enough ropes, there is a crossover temperature above which the behaviour changes to a more pronounced decrease of the critical current. This can be appreciated in figure 4, where we have represented the critical current that would correspond to a thin rope with $n = 2$ and length $L = 425/k_c$. In that case, the critical current at zero temperature would be $2I_c(0) \approx 0.009$ μA (times $2G_1G_2$). Most remarkably, an inflection point is observed in the dependence on temperature. On physical grounds, such a crossover temperature marks the point above which the thermal effects begin to affect significantly the propagation of the Cooper pairs, inducing the pronounced decrease of the supercurrent.

The crossover temperature for the critical current is always found below a scale which is of the order of $\sim v_F/k_B L$. This is perfectly consistent with the behaviour of the 1.7 μm long rope described in [11], where an inflection point can be seen in the plot of the critical current as a function of the temperature. We have represented in figure 5 the results for the critical current computed from (27), for $n = 60$ and $L = 425/k_c$. Comparing with the experimental results in [11], we find that there is a qualitative agreement between the measurements of the critical current for the 1.7 μm long rope and the corresponding plot with the inflection point in figure 5. The temperature dependence in the latter is somewhat smoother, while the experimental results show a more pronounced drop, with the critical current at the transition temperature of the contacts falling to about one quarter of the value at zero temperature. This should be compared with the value of the critical current at the rightmost part of the curve shown in figure 5. We stress that the discrepancy in the decay of the experimental and the theoretical values of $I_c(T)$ may be the consequence of having disregarded the influence of the superconducting transition of the contacts in the model. We remark however that the position of the inflection point in the figure is in good agreement with that seen in the experimental plot.

Bearing in mind that the temperature is measured in the figure in units of $v_F k_c/k_B \approx 1.2\times10^3$ K, we observe that the inflection point in the curve of $I_c(T)$ corresponds to a crossover temperature $T \approx 0.7$ K, which is very close to the value that can be inferred from the results of [11].

We have also represented in figure 5 the behaviour that should be expected if the thick rope were to be shrunk to a length of $\approx$0.3 μm, keeping the same number of metallic nanotubes. In that case, the critical current at zero temperature could be as large as $nI_c(0) \approx 22.5$ μA (times $2G_1G_2$). In agreement with our preceding discussion, the crossover temperature would be shifted in the shorter sample to $T \sim 5$ K, a value that would be in general larger than the transition temperature of the contacts and would then make the crossover unobservable.

5. Conclusions

In this paper, we have developed a transport approach with the aim of accounting for the properties of the supercurrents measured in carbon nanotubes. Some important features of the critical currents reported in [11] cannot be explained within the conventional picture of the proximity effect. In that framework, the values of the supercurrent at zero temperature are given by the expression $\pi\Delta/eR_N$, where R_N is the normal resistance of the junction. That estimate falls short by a factor of 40, for instance, of reproducing the critical current measured in the 0.3 μm long rope considered in [11]. In the 1D approach that we have adopted, the values of the critical currents are determined instead by the scale of the distance between the superconducting contacts, provided that such a quantity is greater than the coherence length in the superconductors. The theoretical values found in this way are in agreement with the experimental measurements for the two samples where supercurrents have been reported in [11].

Even in a 1D framework, it is possible to give two different descriptions depending on whether the contacts are supposed to be perfectly transmitting or not. In the first case, the decay of the critical current for increasing nanotube length turns out to be independent of the strength of the interactions at low temperatures [30]. Such an instance may not be the most appropriate for describing the experimental conditions of the measurements of the proximity effect described in [11] and [12]. In the latter, no evidence of supercurrents has been found for individual nanotubes with a length of about 0.3 μm, placed between Nb contacts. One may think that the main difference between the conditions of the experiments described in [11] and [12] lies in the fact that, in the former, the samples were made of ropes suspended between the electrodes. Such conditions seem to be determining for the observation of supercurrents, which is supported by the fact that the normal resistances of the junctions were comparable in the two kinds of experiment. This should lead us to conclude that the electron–electron interactions play an important role in the observation of the proximity effect in the above mentioned experiments.

We have consequently adopted the point of view in which the single-particle scattering dominates at the contacts between the nanotubes and the electrodes. In these conditions, the values of the critical current depend significantly on the strength of the Coulomb repulsion and the attractive interaction arising from phonon exchange. In the thinner ropes, the repulsive interaction does not suffer a significant reduction from the electrostatic coupling among a small number of metallic nanotubes, and this explains the comparatively small magnitudes of the supercurrents in those instances. The value of the critical current $I_c \approx 0.1$ μA for the very thin rope reported in [11] is actually dictated by the relatively small distance ($\approx$0.3 μm) between the contacts in that sample. We can foresee that, in a similar rope with only two metallic nanotubes extending over a distance $L \approx 1.7$ μm between superconducting contacts, the value of the critical current should decay to a magnitude of $\sim10^{-2}$ μA.

In the thicker ropes, larger supercurrents are expected as the strength of the Coulomb repulsion is significantly reduced from the interaction among the different metallic nanotubes. On the other hand, it is known that the coupling resistance between tubes in a rope is typically above 1 MΩ, which leads us to assume that the conduction is confined to the individual nanotubes. Then, each metallic nanotube in the rope provides a different channel for the propagation of Cooper pairs, whenever there is good contact with the superconducting electrodes. This condition can be difficult to ensure from an experimental point of view, introducing some uncertainty about the real number of metallic nanotubes that may contribute to carrying the supercurrent. We have seen, in particular, that it is possible to account for the value of the critical current in the thick rope described in [11] by adding the currents for the approximate number of metallic nanotubes in the rope.

Finally, let us remark that we have also given a satisfactory description of the temperature dependence of the critical currents reported in [11]. The steady behaviour of the critical current in the thin rope studied there can be understood as a consequence of the relatively short distance between superconducting contacts for that sample. We have seen that, for sufficiently long nanotubes, it is possible to observe a crossover in temperature from the flat behaviour to a pronounced decay of the critical current, before the transition temperature of the contacts is reached. The crossover has to take place at a temperature which is in general slightly below the scale of $v_{\mathrm{F}}/k_{\mathrm{B}}L$, and it is manifested by the presence of an inflection point in the plot of the critical current as a function of the temperature. Such a feature has actually been seen in the experimental measurements on the 1.7 μm long rope studied in [11]. This comes as a genuine signature of the propagation of Cooper pairs along the nanotubes, and stresses once again the suitability of the transport approach for accounting for the unconventional properties observed in the carbon nanotubes.

References

[1] Hamada N, Sawada S and Oshiyama A 1992 *Phys. Rev. Lett.* **68** 1579
[2] Saito R, Fujita M, Dresselhaus G and Dresselhaus M S 1992 *Appl. Phys. Lett.* **60** 2204
[3] Mintmire J W, Dunlap B I and White C T 1992 *Phys. Rev. Lett.* **68** 631
[4] Wildöer J W G, Venema L C, Rinzler A G, Smalley R E and Dekker C 1998 *Nature* **391** 59
[5] Odom T W, Huang J-L, Kim P and Lieber C M 1998 *Nature* **391** 62
[6] See, for instance, González J 2003 Electronic properties of carbon nanotubes *Encyclopedia of Nanoscience and Nanotechnology* ed H S Nalwa (Stevenson Ranch, CA: American Scientific Publishers)
[7] Kane C, Balents L and Fisher M P A 1997 *Phys. Rev. Lett.* **79** 5086
[8] Egger R and Gogolin A O 1997 *Phys. Rev. Lett.* **79** 5082
Egger R and Gogolin A O 1998 *Eur. Phys. J.* B **3** 281
[9] Bockrath M, Cobden D H, Lu J, Rinzler A G, Smalley R E, Balents L and McEuen P L 1999 *Nature* **397** 598
[10] Yao Z, Postma H W Ch, Balents L and Dekker C 1999 *Nature* **402** 273
[11] Kasumov A Yu, Deblock R, Kociak M, Reulet B, Bouchiat H, Khodos I I, Gorbatov Yu B, Volkov V T, Journet C and Burghard M 1999 *Science* **284** 1508
[12] Morpurgo A F, Kong J, Marcus C M and Dai H 1999 *Science* **286** 263
[13] Kociak M, Kasumov A Yu, Guéron S, Reulet B, Khodos I I, Gorbatov Yu B, Volkov V T, Vaccarini L and Bouchiat H 2001 *Phys. Rev. Lett.* **86** 2416
[14] Tang Z K, Zhang L, Wang N, Zhang X X, Wen G H, Li G D, Wang J N, Chan C T and Sheng P 2001 *Science* **292** 2462
[15] González J 2001 *Phys. Rev. Lett.* **87** 136401
[16] González J 2002 *Phys. Rev. Lett.* **88** 076403
[17] Maarouf A A, Kane C L and Mele E J 2000 *Phys. Rev.* B **61** 11156
[18] Stahl H, Appenzeller J, Martel R, Avouris Ph and Lengeler B 2000 *Phys. Rev. Lett.* **85** 5186
[19] González J, Guinea F and Vozmediano M A H 1993 *Nucl. Phys.* B **406** 771
[20] Wang D W, Millis A J and Das Sarma S 2001 *Phys. Rev.* B **64** 193307
[21] Caron L G and Bourbonnais C 1984 *Phys. Rev.* B **29** 4230

[22] Jishi R A, Dresselhaus M S and Dresselhaus G 1993 *Phys. Rev.* B **48** 11385
[23] Sánchez-Portal D, Artacho E, Soler J M, Rubio A and Ordejón P 1999 *Phys. Rev.* B **59** 12678
[24] Woods L M and Mahan G D 2000 *Phys. Rev.* B **61** 10651
[25] Saito R, Jorio A, Souza Filho A G, Dresselhaus G, Dresselhaus M S and Pimenta M A 2002 *Phys. Rev. Lett.* **88** 027401
[26] González J 2003 *Phys. Rev.* B **67** 014528
[27] Alvarez J V and González J 2003 *Phys. Rev. Lett.* at press
[28] Emery V J 1979 *Highly Conducting One-Dimensional Solids* ed J T Devreese, R P Evrard and V E Van Doren (New York: Plenum)
[29] Sólyom J 1979 *Adv. Phys.* **28** 201
[30] Maslov D L, Stone M, Goldbart P M and Loss D 1996 *Phys. Rev.* B **53** 1548
[31] Fazio R, Hekking F W J and Odintsov A A 1996 *Phys. Rev.* B **53** 6653